A smoothed four-node piezoelectric element for analysis of two-dimensional smart structures

H. Nguyen-Van ,*N. Mai-Duy [†]and T. Tran-Cong[‡]

October 21, 2008

Abstract

This paper reports a study of linear elastic analysis of two-dimensional piezoelectric structures using a smoothed four-node piezoelectric element. The element is built by incorporating the strain smoothing method of mesh-free conforming nodal integration into the standard four-node quadrilateral piezoelectric finite element. The approximations of mechanical strains and electric potential fields are normalized using a constant smoothing function. This allows the field gradients to be directly computed from shape functions. No mapping or coordinate transformation is necessary so that the element can be used in arbitrary shapes. Through several examples, the simplicity, efficiency and reliability of the element are demonstrated. Numerical results and comparative studies with other existing solutions in the literature suggest that the present element is robust, computationally inexpensive and easy to implement. textbfkeyword piezoelectric structures, smoothed finite element method, adaptive material, electro-mechanical problems.

1 Introduction

In recent years, there has been a fast growing interest in using piezoelectric materials integrated with structural systems to form a class of smart/intelligent or adaptive structures. Piezoelectric materials have a wide range of engineering applications owing to its inexpensive cost, light weight and the ease with which these materials can be shaped and bonded to surfaces or embedded into structures. The material generates an electric charge under a mechanical load or imposed deformation, which is called the direct piezoelectric effect and conversely, mechanical stress or strain occurs when the material is subjected to an applied electric potential, which is termed as the converse piezoelectric effect. Therefore, piezoelectric materials can be used as sensor (passive) or actuator (active) or both at different times to monitor and actively control vibration, noise and shape of a structural system. They can be also used as a medium to transform electrical and acoustic waves in telecommunication or in an accelerometer.

Significant progress has been made over past decades in analyzing such materials and structures with various approaches, including analytic methods and experimental/numerical models, by many researchers. For example, analytical methods were initially proposed for analysis of beam with piezoelectric patches [Crawley and Luis (1987); Im and Atluri (1989); Shen (1995)] and later for piezoelectric flat panels and plates [Tzou and Tiersten (1994); Bisegna and Maceri (1996); Ray et al. (1998); Lam and Ng (1999), Han et al. (2006), etc.]. However, due to the complexity of governing equations in piezoelectricity, only a few simple problems are solved analytically.

The first significant numerical attempt using finite element implementation for piezoelectric phenomenon was a piezoelectric vibration analysis proposed by Allik and Hughes (1970). Since

*CESRC, Faculty of Engineering & Surveying, USQ, Australia
†CESRC, Faculty of Engineering & Surveying, USQ, Australia
‡CESRC, Faculty of Engineering & Surveying, USQ, Australia

then, the FEM has been considered as a powerful tool for the numerical analysis and design of piezoelectric devices and smart/adaptive structural systems. Most of the finite element models, following the work of Allik and Hughes (see the literature survey of Benjeddou (2000) for example), are based on the interpolation of displacement and electric potential as kinematic field variables that satisfy compatibility equations. These elements are often too stiff, inaccurate and sensitive to mesh distortion. To overcome these shortcomings, hybrid and mixed finite element have been developed, with notable contributions from Cannarozzi and Ubertini (2001) and Sze's group [Sze and Pan (1999); Sze and Yao (2000); Wu et al. (2001); Sze et al. (2004)]. Other relevant works include piezoelectric elements with drilling degrees of freedom of Long et al. (2006); Lim and Lau (2005); Zemcik et al. (2007) . More details and reviews on the development of the finite element methods applied to the modeling and analysis of piezoelectric material and smart structures can be found in Mackerle (2003). So far, many researchers are still actively involved in the development of new special element as can be seen from recent works of Benjeddou (2000); Carrera and Boscolo (2007). However, in the FEM, there often exist difficulties when mesh distortion occurs.

To tolerate mesh distortion in FEM, several recent formulations using mesh-free method have paralleled these developments to simulate piezoelectric structures such as Radial Point Interpolation Meshfree (RIPM) method [Liu et al. (2003)], Point Interpolation Meshfree (PIM) method [Liu et al. (2002)], Point Collocation Meshfree (PCM) method [Ohs and Aluru (2001)], Element Free Galerkin (EFG) method [Liew et al. (2002)], Meshless Local Petrov-Galerkin (MLPG) method [Sladek et al. (2006); Sladek et al. (2007)], etc. Recently, Liu *et al.* [Liu et al. (2007); Liu et al. (2006)] proposed a new smoothed finite element method (SFEM) in which the strain smoothing method (SSM), based on a mesh-free stabilized conforming nodal integration (SCNI), was incorporated into the existing FEM for 2D elastic problems. Further application of SSM for laminated composite plates was presented by Nguyen-Van et al. (2007). It is found that the FEM, integrated with SSM, achieves more accurate results and higher convergence rate as compared with the non-smoothed FEM without increasing the computational cost.

In this study, the SSM is further extended to the analysis of coupling between mechanical and electrical behaviors of two-dimensional piezoelectricity structures. The present smoothed four-node piezoelectric element, named SPQ4, is obtained by incorporating the SSM into the standard four-node quadrilateral piezoelectric element. The approximation of mechanical and dielectric displacements are similar to the conventional finite element method while mechanical strains and electric potential fields are normalized using a constant smoothing function. With the constant smoothing function, domain integrations can be changed into boundary integrations and hence no mapping or coordinate transformation is required in computing the element stiffness matrices. This allows the problem domain discretisation to be more flexible with element shapes. Numerical examples are presented to verify and demonstrate the high performance of the present element. The computed results are also compared with those available from the literature.

The paper is outlined as follows. First, a brief review of the variational form and finite element formulations is introduced in section 2. The description of strain smoothing method for piezoelectric material is derived in section 3. Several numerical applications are investigated in section 4 to assess the performances of the proposed element. Finally, some concluding remarks are withdrawn in the section 5.

2 Variational form and finite element formulations for 2D piezoelectric problems

In this section, the principal equations of piezoelectricity and finite element formulations are briefly reviewed. A two-dimensional piezoelectric problem in domain Ω bounded by Γ is considered. For linear piezoelectric materials, the governing equations and boundary conditions can be derived as

$$\sigma_{ij,i} + f_j = \rho \ddot{u}_j, \tag{1}$$

$$\epsilon_{ij} = \frac{1}{2}(u_{i,j} + u_{j,i}), \tag{2}$$

$$D_{i,i} = 0, \tag{3}$$

$$E_i = -\phi_{,i}, \tag{4}$$

together with the following boundary conditions

$$\sigma_{ij}n_j = \bar{t_i} \quad \text{on} \quad \Gamma_\sigma, \qquad u_i = \bar{u}_i \quad \text{on} \quad \Gamma_u, \tag{5}$$

$$\phi = \bar{\phi} \quad \text{on} \quad \Gamma_\phi, \qquad D_i n_i = -\bar{q} \quad \text{on} \quad \Gamma_q, \tag{6}$$

where σ_{ij}, ϵ_{ij} represent stress and strain tensor respectively, f_j is the body force density, u_j is the mechanical displacement vector, ρ is the mass density, D_i is the dielectric displacement vector, E_i is the electric field vector and ϕ is the scalar electric potential field.

The general functional L is obtained by summing the kinetic energy, strain energy, dielectric energy and potential energy of external fields as follows.

$$L = \int_\Omega \left[\frac{1}{2}\rho\dot{\mathbf{u}}^T\dot{\mathbf{u}} - \frac{1}{2}\boldsymbol{\epsilon}^T\boldsymbol{\sigma} + \frac{1}{2}\mathbf{D}^T\mathbf{E} + \mathbf{u}^T\mathbf{f}\right] d\Omega + \int_\Gamma \left[\mathbf{u}^T\bar{\mathbf{t}} + \phi^T\bar{\mathbf{q}}\right] d\Gamma. \tag{7}$$

Then the variational form of the equations of motion can be derived using Hamilton's principle

$$\int_\Omega [\delta\boldsymbol{\epsilon}^T\boldsymbol{\sigma} + \delta\mathbf{u}^T\rho\ddot{\mathbf{u}} - \delta\mathbf{E}^T\mathbf{D} - \delta\mathbf{u}^T\mathbf{f}]d\Omega - \int_\Gamma [\delta\mathbf{u}^T\bar{\mathbf{t}} + \delta\phi^T\bar{\mathbf{q}}]d\Gamma = 0. \tag{8}$$

The mechanical constitutive relation for 2D piezoelectric materials can be expressed in the e-form as

$$\begin{aligned} \boldsymbol{\sigma} &= \mathbf{c}_E\boldsymbol{\epsilon} - \mathbf{e}^T\mathbf{E}, \\ \mathbf{D} &= \mathbf{e}\boldsymbol{\varepsilon} + \mathbf{g}\mathbf{E}, \end{aligned} \tag{9}$$

where $\mathbf{c}_E$ is the elastic stiffness matrix for constant electric field, $\mathbf{e}$ is the piezoelectric matrix and $\mathbf{g}$ is the dielectric constant matrix for constant mechanical strain.

Equation (9) can be rewritten in the explicit form in the $x-z$ plane as

$$\begin{bmatrix} \sigma_x \\ \sigma_z \\ \tau_{xz} \end{bmatrix} = \begin{bmatrix} c_{11} & c_{13} & 0 \\ c_{13} & c_{33} & 0 \\ 0 & 0 & c_{55} \end{bmatrix} \begin{bmatrix} \epsilon_x \\ \epsilon_z \\ \gamma_{xz} \end{bmatrix} - \begin{bmatrix} 0 & e_{31} \\ 0 & e_{33} \\ e_{15} & 0 \end{bmatrix} \begin{bmatrix} E_x \\ E_z \end{bmatrix}, \tag{10}$$

$$\begin{bmatrix} D_x \\ D_z \end{bmatrix} = \begin{bmatrix} 0 & 0 & e_{15} \\ e_{31} & e_{33} & 0 \end{bmatrix} \begin{bmatrix} \epsilon_x \\ \epsilon_z \\ \gamma_{xz} \end{bmatrix} - \begin{bmatrix} g_{11} & 0 \\ 0 & g_{33} \end{bmatrix} \begin{bmatrix} E_x \\ E_z \end{bmatrix}. \tag{11}$$

If the piezoelectric stress constants are unavailable in Equation (10) or (11), they can be obtained by using the following relationship

$$\begin{bmatrix} 0 & 0 & e_{15} \\ e_{31} & e_{33} & 0 \end{bmatrix} = \begin{bmatrix} 0 & 0 & d_{15} \\ d_{31} & d_{33} & 0 \end{bmatrix} \begin{bmatrix} c_{11} & c_{13} & 0 \\ c_{13} & c_{33} & 0 \\ 0 & 0 & c_{55} \end{bmatrix}. \tag{12}$$

in which $[d]$ is the piezoelectric strain constant matrix.

The finite element approximation solution for 2D piezoelectric problems using the standard 4-node quadrilateral element can be expressed as

$$\mathbf{u} = \mathbf{N}_u \mathbf{u}^e, \tag{13}$$

$$\boldsymbol{\phi} = \mathbf{N}_\phi \boldsymbol{\phi}^e, \tag{14}$$

where $\mathbf{u}^e$ and $\boldsymbol{\phi}^e$ are the nodal displacement and nodal electric potential vectors, $\mathbf{N}_u$ and $\mathbf{N}_\phi$ are shape function matrices. They are given by

$$\mathbf{u}^e = \sum_{i=1}^{4} [u_i \quad v_i], \tag{15}$$

$$\boldsymbol{\phi}^e = \sum_{i=1}^{4} [\phi_i], \tag{16}$$

$$\mathbf{N}_u = \begin{bmatrix} N_i & 0 \\ 0 & N_i \end{bmatrix}, \tag{17}$$

$$\mathbf{N}_\phi = [N_i], \tag{18}$$

in which $N_i = \frac{1}{4}(1+\xi_i\xi)(1+\eta_i\eta)$ is the bilinear shape function of the four-node serendipity element.

The corresponding approximation of the linear strain $\boldsymbol{\epsilon}$ and electric field $\mathbf{E}$ are

$$\boldsymbol{\epsilon} = \nabla_s \mathbf{u} = \mathbf{B}_u \mathbf{u}^e, \tag{19}$$

$$\mathbf{E} = -\nabla\phi = \mathbf{B}_\phi \boldsymbol{\phi}^e, \tag{20}$$

where

$$\mathbf{B}_u = \begin{bmatrix} N_{i,x} & 0 \\ 0 & N_{i,z} \\ N_{i,z} & N_{i,x} \end{bmatrix}, \tag{21}$$

$$\mathbf{B}_\phi = \begin{bmatrix} N_{i,x} \\ N_{i,z} \end{bmatrix}. \tag{22}$$

Substituting Equations (19)–(22) into Equation (8) leads to the piezoelectric dynamic equations

$$\begin{bmatrix} \mathbf{M}^e_{uu} & 0 \\ 0 & 0 \end{bmatrix} \begin{Bmatrix} \ddot{\mathbf{u}} \\ \ddot{\boldsymbol{\phi}} \end{Bmatrix} + \begin{bmatrix} \mathbf{K}^e_{uu} & \mathbf{K}^e_{u\phi} \\ \mathbf{K}^e_{u\phi} & \mathbf{K}^e_{\phi\phi} \end{bmatrix} \begin{Bmatrix} \mathbf{u} \\ \boldsymbol{\phi} \end{Bmatrix} = \begin{Bmatrix} \mathbf{F} \\ \mathbf{Q} \end{Bmatrix}, \tag{23}$$

in which

$$\mathbf{M}^e_{uu} = \int_\Omega \rho \mathbf{N}_u^T \mathbf{N}_u d\Omega, \tag{24}$$

$$\mathbf{K}^e_{uu} = \int_\Omega \mathbf{B}_u^T \mathbf{c}_E \mathbf{B}_u d\Omega, \tag{25}$$

$$\mathbf{K}^e_{u\phi} = \int_\Omega \mathbf{B}_u^T \mathbf{e}^T \mathbf{B}_\phi d\Omega, \tag{26}$$

$$\mathbf{K}^e_{\phi\phi} = -\int_\Omega \mathbf{B}_\phi^T \mathbf{g} \mathbf{B}_\phi d\Omega, \tag{27}$$

$$\mathbf{F} = \int_\Omega \mathbf{N}_u^T \mathbf{f} d\Omega + \int_{\Gamma_\sigma} \mathbf{N}_u^T \bar{\mathbf{t}} d\Gamma, \tag{28}$$

$$\mathbf{Q} = \int_{\Gamma_q} \mathbf{N}_\phi^T \bar{\mathbf{q}} d\Gamma. \tag{29}$$

3 Strain smoothing approach for piezoelectric finite element method

The smoothed strain and smoothed electric field at an arbitrary point $\mathbf{x}_C$ are obtained by

$$\tilde{\boldsymbol{\epsilon}}(\mathbf{x}_C) = \int_{\Omega_C} \boldsymbol{\epsilon}(\mathbf{x}) \Phi(\mathbf{x} - \mathbf{x}_C) d\Omega, \tag{30}$$

$$\tilde{\mathbf{E}}(\mathbf{x}_C) = \int_{\Omega_C} \mathbf{E}(\mathbf{x}) \Phi(\mathbf{x} - \mathbf{x}_C) d\Omega, \tag{31}$$

where $\boldsymbol{\epsilon}$, $\mathbf{E}$ are respectively the mechanical strain and electric field obtained from displacement compatibility condition as given in Equations (19) and (20). Ω_C is the smoothing cell domain on which the smoothing operation is performed. Depending on the stability analysis [Liu et al. (2007); Liu et al. (2006)], Ω_C may be an entire element or part of an element as shown in Figure 1. Φ is a smoothing function that satisfies the following properties

$$\Phi \geq 0 \qquad \text{and} \qquad \int_\Omega \Phi \mathrm{d}\Omega = 1. \tag{32}$$

For simplicity, Φ is chosen as a constant function

$$\Phi(\mathbf{x} - \mathbf{x}_C) = \begin{cases} 1/A_C & \mathbf{x} \in \Omega_C, \\ 0 & \mathbf{x} \notin \Omega_C. \end{cases} \tag{33}$$

where $A_C = \int_{\Omega_C} d\Omega$ is the area of the smoothing cell (subcell).

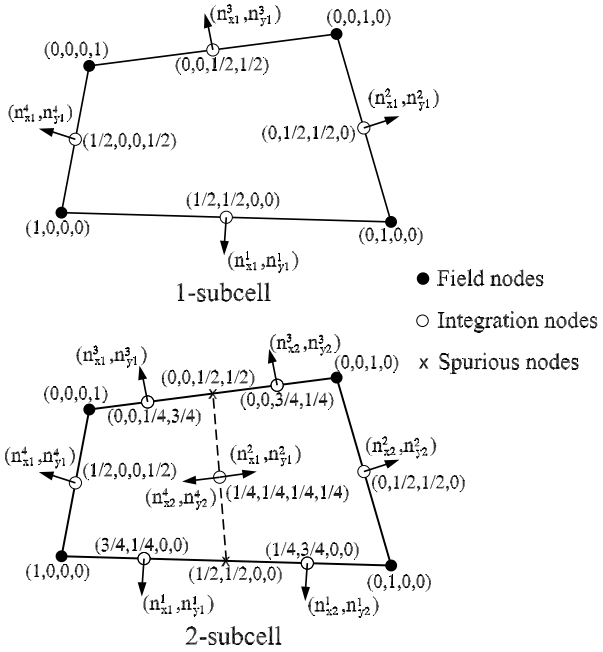

Figure 1: Subdivision of an element into smoothing cells (nc) and the values of shape functions at nodes.

Substituting Φ into Equations (30)–(31) and applying the divergence theorem, we obtain the smoothed strain and smoothed electric field in the domain Ω_C as follows.

$$\tilde{\boldsymbol{\epsilon}}(\mathbf{x}_C) = \frac{1}{A_C} \int_{\Omega_C} \nabla_s \mathbf{u}(\mathbf{x}) d\Omega = \frac{1}{A_C} \int_{\Gamma_C} \mathbf{n}_u \mathbf{u}(\mathbf{x}) d\Gamma, \tag{34}$$

$$\tilde{\mathbf{E}}(\mathbf{x}_C) = -\frac{1}{A_C} \int_{\Omega_C} \nabla \boldsymbol{\phi}(\mathbf{x}) d\Omega = -\frac{1}{A_C} \int_{\Gamma_C} \mathbf{n}_\phi \boldsymbol{\phi}(\mathbf{x}) d\Gamma, \tag{35}$$

where $\mathbf{n}_u$ and $\mathbf{n}_\phi$ are outward normal matrices on the boundary Γ_C

$$\mathbf{n}_u = \begin{bmatrix} n_x & 0 \\ 0 & n_z \\ n_z & n_x \end{bmatrix}, \quad \mathbf{n}_\phi = [n_x \quad n_z]^T. \tag{36}$$

Introducing the finite element approximation of $\mathbf{u}$ and $\boldsymbol{\phi}$ into Equations (34) and (35) one gets

$$\tilde{\boldsymbol{\epsilon}}(\mathbf{x}_C) = \sum_{i=1}^{nc} \tilde{\mathbf{B}}_{ui}(\mathbf{x}_C) \mathbf{u}^e, \tag{37}$$

$$\tilde{\mathbf{E}}(\mathbf{x}_C) = -\sum_{i=1}^{nc} \tilde{\mathbf{B}}_{\phi i}(\mathbf{x}_C) \boldsymbol{\phi}^e, \tag{38}$$

in which

$$\tilde{\mathbf{B}}_{ui}(\mathbf{x}_C) = \frac{1}{A_C}\int_{\Gamma_C}\begin{bmatrix} N_i n_x & 0 \\ 0 & N_i n_z \\ N_i n_z & N_i n_x \end{bmatrix} d\Gamma, \tag{39}$$

$$\tilde{\mathbf{B}}_{\phi i}(\mathbf{x}_C) = \frac{1}{A_C}\int_{\Gamma_C}\begin{bmatrix} N_i n_x \\ N_i n_z \end{bmatrix} d\Gamma. \tag{40}$$

Using one Gaussian point to evaluate Equation (39) and (40) along each line segment of the boundary Γ_i^C of Ω_C, they can be transformed as

$$\tilde{\mathbf{B}}_{ui}(\mathbf{x}_C) = \frac{1}{A_C}\sum_{b=1}^{nb}\begin{bmatrix} N_i(\mathbf{x}_b^G) n_x & 0 \\ 0 & N_i(\mathbf{x}_b^G) n_z \\ N_i(\mathbf{x}_b^G) n_z & N_i(\mathbf{x}_b^G) n_x \end{bmatrix} l_b^C, \tag{41}$$

$$\tilde{\mathbf{B}}_{\phi i}(\mathbf{x}_C) = \frac{1}{A_C}\sum_{b=1}^{nb}\begin{bmatrix} N_i(\mathbf{x}_b^G) n_x \\ N_i(\mathbf{x}_b^G) n_z \end{bmatrix} l_b^C, \tag{42}$$

where $\mathbf{x}_b^G$ and l_b^C are the midpoint (Gauss point) and the length of Γ_b^C, respectively; nb is the total number of edges of each smoothing cell.

Finally, the linear equations of motion (23) can be rewritten as follows

$$\begin{bmatrix} \mathbf{M}_{uu}^e & 0 \\ 0 & 0 \end{bmatrix}\begin{Bmatrix} \ddot{\mathbf{u}} \\ \ddot{\boldsymbol{\phi}} \end{Bmatrix} + \begin{bmatrix} \tilde{\mathbf{K}}_{uu}^e & \tilde{\mathbf{K}}_{u\phi}^e \\ \tilde{\mathbf{K}}_{u\phi}^e & \tilde{\mathbf{K}}_{\phi\phi}^e \end{bmatrix}\begin{Bmatrix} \mathbf{u} \\ \boldsymbol{\phi} \end{Bmatrix} = \begin{Bmatrix} \mathbf{F} \\ \mathbf{Q} \end{Bmatrix}, \tag{43}$$

where

$$\tilde{\mathbf{K}}_{uu}^e = \sum_{C=1}^{nc}\tilde{\mathbf{B}}_{uC}^T \mathbf{c}_E \tilde{\mathbf{B}}_{uC} A_C, \tag{44}$$

$$\tilde{\mathbf{K}}_{u\phi}^e = \sum_{C=1}^{nc}\tilde{\mathbf{B}}_{uC}^T \mathbf{e}^T \tilde{\mathbf{B}}_{\phi C} A_C, \tag{45}$$

$$\tilde{\mathbf{K}}_{\phi\phi}^e = -\sum_{C=1}^{nc}\tilde{\mathbf{B}}_{\phi C}^T \mathbf{g}^T \tilde{\mathbf{B}}_{\phi C} A_C. \tag{46}$$

Equation (43) forms the basis of the smoothed piezoelectric finite element method. In this work, four-node quadrilateral element is employed for domain discretization. Two smoothing cells or subcells ($nc = 2$) are used to evaluate Equation (44)–(46). Further increase of nc will lead to high computational cost but the accuracy may not be better because this results in stiffer system [Liu et al. (2006)]. The obtained four-node piezoelectric element with two smoothing cells is named SPQ4 (Smoothed Piezoelectric Quadrilateral 4-node element).

4 Numerical results

In this section, several numerical examples are employed to test and assess the performance of the SPQ4 element as applied to the linear static and free vibration analysis of two-dimensional piezoelectric structures.

4.1 Patch testing

The patch test is an essential check for convergence and is used to verify whether the element can display exactly the constitutive behaviour of material through correct stresses, when subjected to constant strains. In this section, a patch test is used to verify that our proposed element, SPQ4, has proper convergence properties. A choice of material, mesh and boundary conditions was adopted from the work of Sze et al. (2004), as shown in Figure 2.

The following PZT4 material in reference Sze et al. (2004) is used for the patch test.
$c_{11} = 139 \times 10^3$, $c_{33} = 113 \times 10^3$, $c_{13} = 74.3 \times 10^3$, $c_{55} = 25.6 \times 10^3 (N/mm^2)$,

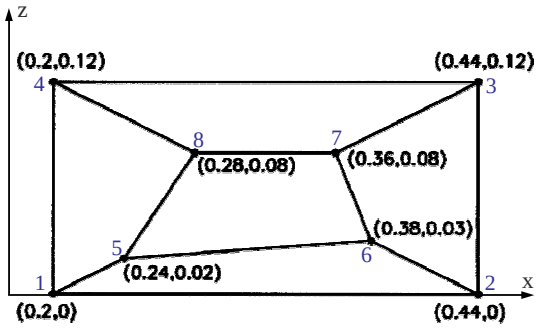

Figure 2: Geometry and mesh of the piezoelectric patch test.

$e_{15} = 13.44 \times 10^6$, $e_{31} = -6.98 \times 10^6$, $e_{33} = 13.84 \times 10^6$ (pC/mm^2),
$g_{11} = 6.00 \times 10^9$, $g_{33} = 5.47 \times 10^9$ $(pC/GVmm)$.

The prescribed mechanical displacements and electric potentials are applied at the edges defined by nodes 1, 2, 3 and 4 as follows.

$$u_x = s_{11}\sigma_0 x, \quad u_z = s_{13}\sigma_0 z, \quad \phi = b_{31}\sigma_0 z.$$

where $\sigma_0 = 1000$ is an arbitrary stress parameter. s_{11}, s_{13} and b_{31} are material constants which can be calculated by the following relation

$$\begin{bmatrix} s_{11} & s_{13} & g_{31} \\ s_{13} & s_{33} & b_{33} \\ b_{31} & b_{33} & -f_{33} \end{bmatrix} = \begin{bmatrix} c_{11} & c_{13} & e_{31} \\ c_{13} & c_{33} & e_{33} \\ e_{31} & e_{33} & -g_{33} \end{bmatrix}^{-1}.$$

Under the boundary conditions described above, the corresponding exact stress $\boldsymbol{\sigma}$ and electric displacement $\mathbf{D}$ are given as

$$\sigma_x = \sigma_0, \quad \sigma_z = \tau_{xz} = D_x = D_z = 0.$$

As expected, the obtained results using SPQ4 elements match the exact solution as shown in Table 1 and hence SPQ4 elements successfully passed the patch test.

4.2 Single-layer piezoelectric strip in shear deformation

This example considers the shear deformation of a 1×1 mm single-layer square strip (Figure 3), polarized in the $z-$direction as proposed in Ohs and Aluru (2001). The material PZT-5 was used for this problem. Their properties and other important values are summarized in Table 2.

The strip is subjected to a uniform compressive stress σ_0 in the z direction and an applied voltage V_0 as shown on Figure 3. The applied electric field is perpendicular to the polarization of the material to cause a shear strain in the strip. The overall deformation is a superposition of the deformation due to the shear strain and the compressive load. The following mechanical and electrical boundary conditions were applied to the sides of the strip

$$\begin{array}{lll} \phi_{,z}(x,\pm h) = 0, & \sigma_z(x,\pm h) = \sigma_0, & \tau_{xz}(L,z) = 0, \\ \tau_{xz}(x,\pm h) = 0, & \phi(L,z) = -V_0, & \sigma_x(L,z) = 0, \\ \phi(0,z) = +V_0, & u(0,z) = 0, \quad w(0,0) & = 0. \end{array}$$

The analytical solution for this problem is given by Gaudnzi and Bathe (1995)

$$\begin{aligned} u &= s_{13}\sigma_0 x, \\ w &= \frac{d_{15}V_0 x}{h} + s_{33}\sigma_0 z, \\ \phi &= V_0\left(1 - 2\frac{x}{L}\right). \end{aligned}$$

Table 1: Results of the patch test.

Variable	Results	
	SPQ4	Exact
σ_x	1000	1000
σ_z	1.9397×10^{-10}	0
τ_{xz}	9.4022×10^{-11}	0
D_x	9.1261×10^{-8}	0
D_z	-1.4486×10^{-8}	0
u_{x5}	1.9012×10^{-3}	1.9012×10^{-3}
u_{z5}	-6.0626×10^{-5}	-6.0626×10^{-5}
ϕ_5	-3.5557×10^{-7}	-3.5557×10^{-7}
u_{x6}	3.0103×10^{-3}	3.0103×10^{-3}
u_{z6}	-9.0939×10^{-5}	-9.0939×10^{-5}
ϕ_6	-5.3335×10^{-7}	-5.3335×10^{-7}
u_{x7}	2.8519×10^{-3}	2.8519×10^{-3}
u_{z7}	-2.4251×10^{-4}	-2.4251×10^{-4}
ϕ_7	-1.4223×10^{-6}	-1.4223×10^{-6}
u_{x8}	2.2181×10^{-3}	2.2181×10^{-3}
u_{z8}	-2.4251×10^{-4}	-2.4251×10^{-4}
ϕ_8	-1.4223×10^{-6}	-1.4223×10^{-6}

Table 2: Single-layer piezoelectric material properties, dimensions and other constants.

s_{11}	$16.4 \times 10^{-6} \frac{(mm)^2}{N}$	d_{31}	$-172 \times 10^{-9} \frac{mm}{V}$
s_{13}	$-7.22 \times 10^{-6} \frac{(mm)^2}{N}$	d_{33}	$-374 \times 10^{-9} \frac{mm}{V}$
s_{33}	$18.8 \times 10^{-6} \frac{(mm)^2}{N}$	d_{15}	$584 \times 10^{-9} \frac{mm}{V}$
s_{55}	$47.5 \times 10^{-6} \frac{(mm)^2}{N}$	g_{11}	$1.53105 \times 10^{-8} \frac{N}{V^2}$
σ_0	$-5.0 \frac{N}{mm^2}$	g_{33}	$1.505 \times 10^{-8} \frac{N}{V^2}$
σ_1	$20.0 \frac{N}{mm^2}$	V_0	$1000V$
L	$1.0mm$	h	$0.5mm$

To demonstrate the capability of the SPQ4 elements with various complex shapes, the strip is modelled with two types of mesh in this analysis with 10×10 regular as well as irregular elements as shown in Figure 4.

A plot of the total deformation of the strip is presented in Figure 5. The total displacements obtained with regular and irregular mesh are compared and plotted together with exact solutions in Figure 6 and Figure 7. Note that the computed displacements u are along the right side ($x = L$) while the displacements w distribute along the bottom edge ($z = -h$). The distribution of the computed electric potentials along the bottom side ($z = -h$) is also demonstrated in Figure 8. It is observed that all the computed displacements and electric potentials for both types of mesh are in excellent agreement with the analytical solutions.

4.3 Single-layer piezoelectric strip in bending

The strip with the same material and geometry as in the previous example is considered but with modified boundary conditions for bending situation. In this case, the top and bottom surfaces are poled and electroded in the same direction to cause the strip contracting in the $z-$direction and expanding along the $x-$direction. The strip also bends downward due to the linear applied stress at the right edge as shown in Figure 9.

The following mechanical and electrical boundary conditions are applied to the edges of the

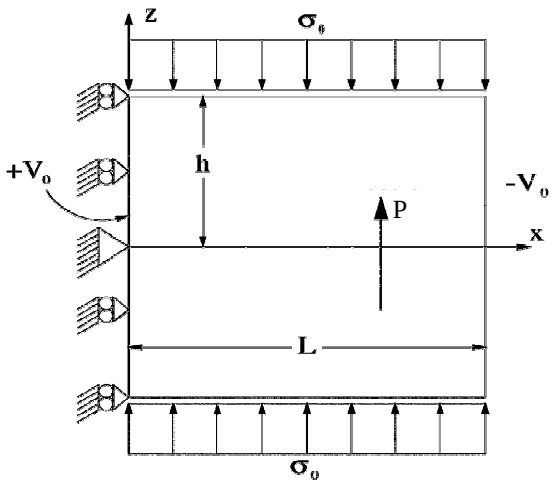

Figure 3: Piezo-strip subjected to a uniform stress and an applied voltage.

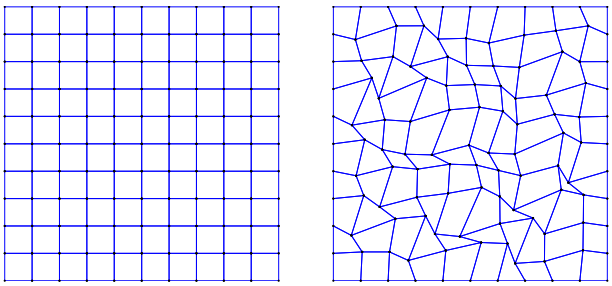

(a) regular elements (b) irregular elements

Figure 4: Typical meshes of the single-layer piezoelectric strip.

strip

$$\begin{aligned} \phi(x,\pm h) = \pm V_0, \quad \sigma_z(x,\pm h) = 0, \quad \tau_{xz}(x,\pm h) = 0, \\ \phi_{,x}(L,z) = 0, \quad \sigma_x(L,z) = \sigma_0 + \sigma_1 z, \quad \tau_{xz}(L,z) = 0, \\ \phi_{,x}(0,z) = 0, \qquad u(0,z) = 0, \quad w(0,0) = 0. \end{aligned}$$

The analytical solution is available for this problem and can be found in Gaudnzi and Bathe (1995); Ohs and Aluru (2001) as follows

$$\begin{aligned} u &= s_{11}\left(\sigma_0 - \frac{d_{31}V_0}{s_{11}h}\right) + s_{11}\left(1 - \frac{d_{31}^2}{s_{11}g_{33}}\right)\sigma_1 xz, \\ w &= s_{13}\left(\sigma_0 - \frac{d_{33}V_0}{s_{13}h}\right) z + s_{13}\left(1 - \frac{d_{33}d_{31}}{s_{13}g_{33}}\right)\sigma_1 \frac{z^2}{2} \\ &\quad -s_{11}\left(1 - \frac{d_{31}^2}{s_{11}g_{33}}\right)\sigma_1 \frac{x^2}{2}, \\ \phi &= V_0 \frac{z}{h} - \frac{d_{31}\sigma_1}{2g_{33}}(h^2 - z^2). \end{aligned}$$

Two types of mesh as shown in Figure 4 are analyzed again. The obtained deformation of the strip is shown in Figure 10. Figure 11 illustrates the computed and exact displacements u along the right side ($x = L$) while the vertical displacements w along the bottom edge ($z = -h$) are shown in Figure 12. The distribution of the computed electric potentials along the right side ($x = L$) with the exact solution are demonstrated in Figure 13. Once again, both computed displacements and electric potential match well the exact solutions for regular mesh as well as for highly distorted mesh.

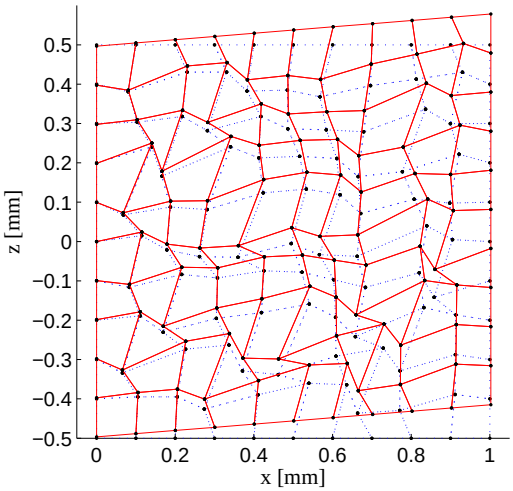

Figure 5: Total deformation of the strip in shearing.

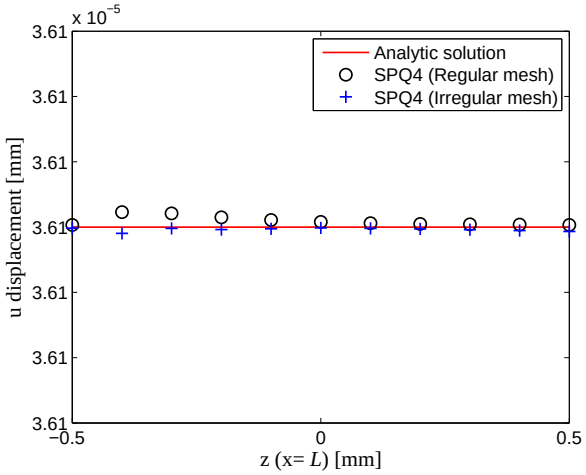

Figure 6: Computed and exact $u-$displacements.

4.4 A parallel piezoelectric bimorph beam

The example to be discussed here is the two-layer parallel bimorph beam. It consists of a cantilever piezoelectric beam made of two PVDF layers of the same thickness $h_t = h_b = H/2 = 0.2$ mm and a length of $L = 5$ mm, with same polarization orientations as shown in Figure 14. The PVDF material properties are summarized as follows $E = 2 \quad GPa, \nu = 0.29, e_{31} = 0.046 \quad C/m^2, \quad e_{32} = 0.046 \quad C/m^2, g_{11} = 0.1062 \times 10^{-9} \quad F/m, \quad g_{33} = 0.1062 \times 10^{-9} \quad F/m$.

For the parallel bimorph configuration, a zeros voltage ($V = 0$) is applied to the intermediate electrode, while the voltage $V = 1$ is applied to the bottom and top faces of the beam so that the electric field along the thickness direction across the lower and upper layers are in opposite direction. This will generate moments that bend the bimorph.

In this study, the beam is assumed to be in a plane stress state. For an applied electric field V only, the tip deflection δ of the cantilever parallel bimorph can be approximated as [Cambridge (1995)]

$$\delta = \frac{2L^2 V d_{31}}{H^2}. \tag{47}$$

With $L = 5$ mm and $H = 0.4$ mm, the approximated value of the tip deflection calculated from Equation (47) is $\delta = 1.0206 \times 10^{-8}$ (m).

The beam is analyzed using 15×2, 25×2, 35×2 and 50×2 meshes of SPQ4 elements. Table 3 presents the obtained tip deflections together with analytic and meshless solutions such as PIM

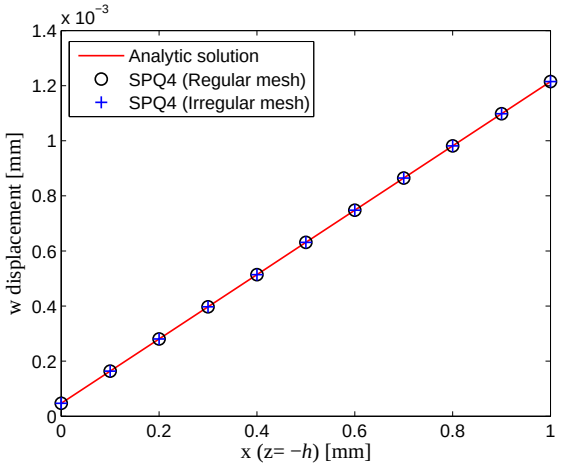

Figure 7: Computed and exact $w-$displacements.

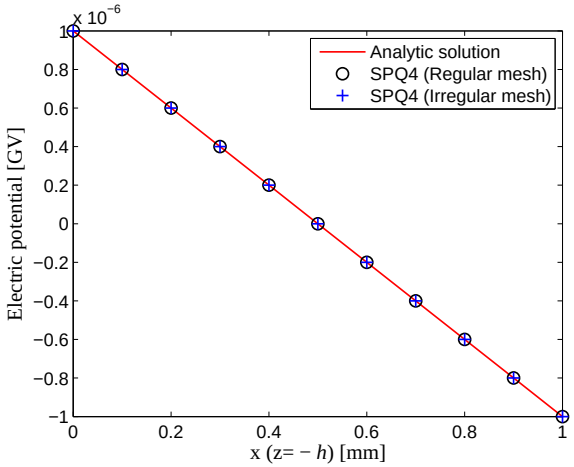

Figure 8: Computed and exact electric potential ϕ.

[Liu et al. (2002)] and RPIM [Liu et al. (2003)]. Note that the values in parentheses corresponding to the percentage of relative error compared with analytic solutions. It can be seen that the present element, SPQ4, gives more accurate results than those of other numerical solutions cited here. A plot of the total mechanical deformation of the bimorph with 25×2 mesh is also given in Figure 15.

4.5 A piezoelectric Cook's membrane

This section deals with a clamped tapered panel with distributed in-plane tip load $F = 1$ similar to the well-known Cook's membrane. The lower surface is subjected to a voltage $V = 0$. The geometry and boundary conditions of the beam are shown in the Figure 16. The beam is made of PZT4 material as in the section 4.1.

Since no analytic solution is available for this problem, the present results are compared with a finite element solution with a fine mesh. The best known values of the displacement, the electric potential, the first principal stress and the electric flux density at node A, B, C respectively, according to Long et al. (2006) are
$u_{zA} = 2.109 \times 10^{-4} mm, \phi_A = 1.732 \times 10^{-8} GV,$
$\sigma_{1B} = 0.21613 N/mm^2, D_C = 22.409 pC/mm^2.$

Table 4 presents the obtained results with mesh refinement and relative error (values in parentheses) when compared with the best known values using a fine mesh of FEM [Long et al. (2006)]. It can be seen that relative errors reduce when the mesh is refined. With a mesh of 24×24 elements, the present method achieves excellent accuracy on displacement u_{zA} (relative error= 0.379%) and

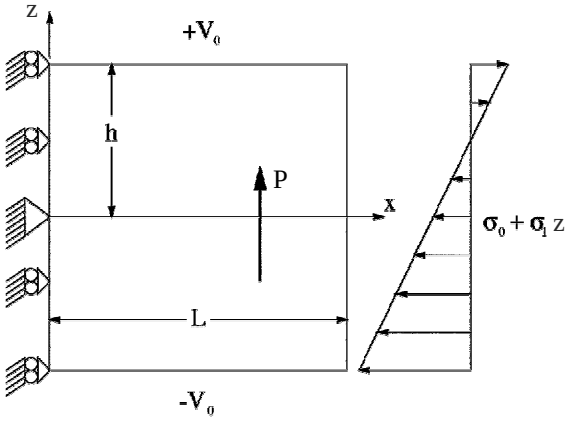

Figure 9: Piezo-strip subjected to a linear stress and an applied voltage.

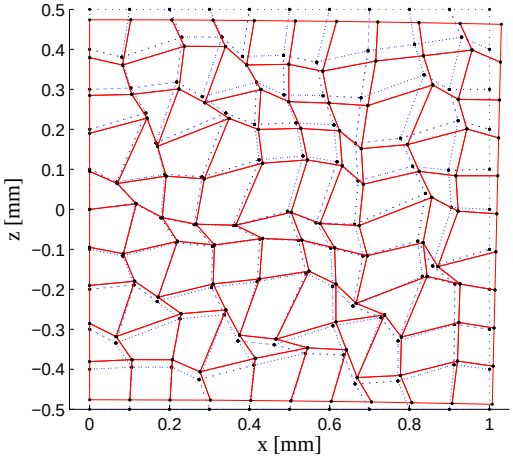

Figure 10: Total deformation of the strip in bending.

reasonable predictions for ϕ_A, σ_{1B} as well as D_{1C}.

4.6 Free vibration of a piezoelectric transducer

This section performs an eigenvalue analysis of a piezoelectric transducer consisting of a piezoelectric wall made of PZT4 material as in the section 4.1 with brass end caps as shown in Figure 17. The piezoelectric material is electroded on both the inner and outer surfaces. This problem is similar to the one studied numerically by Liu et al. (2003) and experimentally by Mercer et al. (1987).

The transducer is modeled as an axisymmetric structures with 44 SPQ4 elements as shown in Figure 18. The obtained results are compared with those of Liu et al. (2002) using PIM method and experimental results reported in Mercer et al. (1987) as given in Table 5. The values in parentheses correspond to the relative error compared with experimental results. It can be seen that the present solutions in general indicate good agreement with experimental results and give smaller relative error than those of PIM results. The first four mode shapes are also displayed in Figure 19 which are identical to those depicted in Liu et al. (2003).

5 Conclusions

A simple and efficient four-node quadrilateral piezoelectric element SPQ4 has been developed and reported in this paper for linear analysis of two-dimensional piezoelectric problems. Both static and free vibration analysis are considered. The element is obtained by incorporating cell-wise strain smoothing method into the standard FEM. This technique allows field gradients to be computed directly from shape functions themselves (i.e. derivatives of shape functions are not required) and

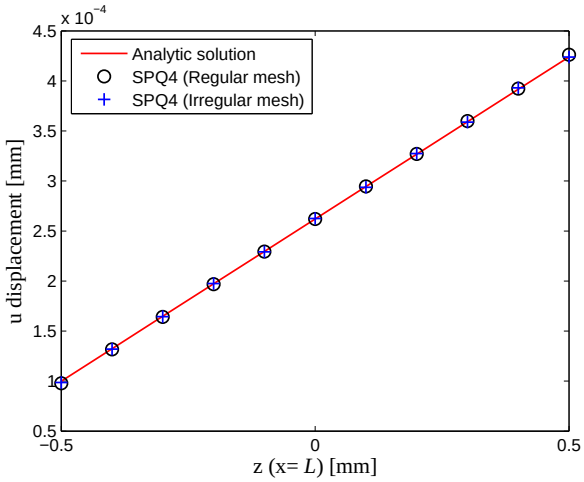

Figure 11: Computed and exact $u-$displacements.

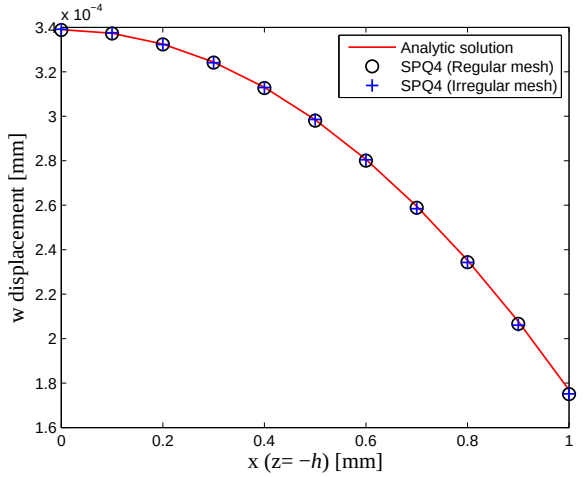

Figure 12: Computed and exact $w-$displacements.

hence no limitation is imposed on the shape of elements. Domain discretization is therefore more flexible than in the case of the standard FEM. Moreover, these good features are acquired without increasing the number of field nodes and computational cost. The changes to the existing finite element code are also very small. Several numerical examples are studied and the obtained results are in excellent agreement with analytical solutions. It is found that the SPQ4 element is robust and reliable. It can yield reasonable results even with coarse discretization.

acknowledgement The first author is supported by the Faculty of Engineering and Surveying (FoES) and the Computational Engineering & Science Research Center (CESRC), USQ, Australia. These supports are gratefully acknowledged.

References

Allik, H. and Hughes, T. (1970). Finite element method for piezoelectric vibration, *International Journal for Numerical Methods in Engineering* **2**: 151–157.

Benjeddou, A. (2000). Advances in piezoelectric finite element modeling of adaptive structural elements: a survey, *Computers and Structures* **76**: 347–363.

Bisegna, P. and Maceri, F. (1996). An exact three-dimensional solution for simply supported rectangular piezoelectric plate, *ASME Journal of Applied Mechanics* **63**: 628–638.

Cambridge, M. (1995). *Product Catalogue: Piezo Systems Inc.*, cambridge ma edn.

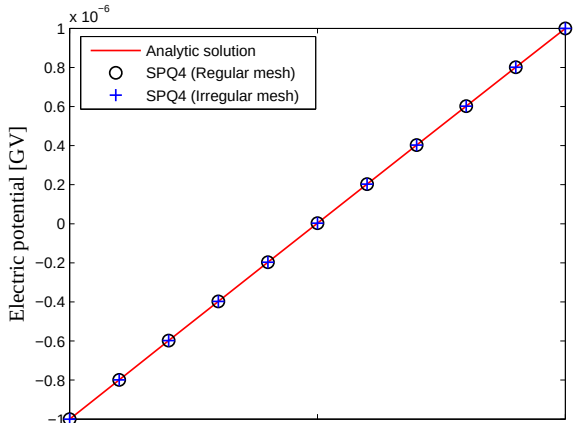

Fig

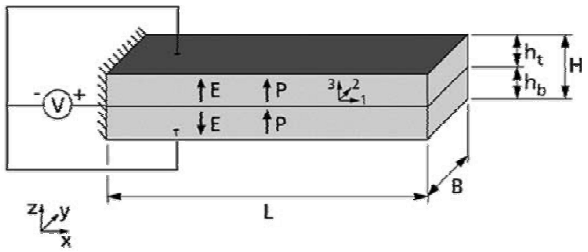

Figure 14: Two-layer parallel bimorph cantilever beam.

Cannarozzi, A. and Ubertini, F. (2001). Some hybrid variational methods for linear electroelasticity problems, *International Journal of Solids and Structures* **38**: 2573–2596.

Carrera, E. and Boscolo, M. (2007). Classical and mixed finite elements for static and dynamic analysis of piezoelectric plates, *International Journal for Numerical Methods in Engineering* **70**: 1135–1181.

Crawley, E. F. and Luis, J. D. (1987). Use of piezoelectric actuators as elements of intelligent strucutures, *AIAA Journall* **25**: 1373–1385.

Gaudnzi, P. and Bathe, K. J. (1995). An iterative finite element procedure for the analysis of piezoelectric continua, *Journal of Intelligent Material System Structures* **6**: 266–273.

Han, F., Pan, E., Roy, A. K. and Yue, Z. Q. (2006). Responses of Piezoelectric, Transversely Isotropic, Functionally Graded, and Multilayered Half Spaces to Uniform Circular Surface Loadings, *CMES: Computer Modeling in Engineering & Sciences* **14**(1): 15–30.

Im, S. and Atluri, S. N. (1989). Effect of a piezo-actuator on a finitely deformed beam subjected to general loading, *AIAA Journal* **27**: 1801–1807.

Lam, K. Y. and Ng, T. Y. (1999). Active control of composite plates with integrated piezoelectric sensors and actuators under various dynamic loading conditions, *Smart Materials and Structures* **8**: 223–237.

Liew, K. M., Lim, H. K., Tan, M. J. and He, X. Q. (2002). Analysis of laminated composite beams and plates with piezoelectric patches using the element-free Galerkin method, *Computational Mechanics* **29**: 486–497.

Lim, C. W. and Lau, C. W. H. (2005). A new two-dimensional model for electro-mechanical response of thick laminated piezoelectric actuator, *International Journal of Solids and Structures* **42**: 5589–5611.

Table 3: Tip deflections of the bimorph beam and comparison with available literatures ($\times 10^{-8}$ m).

Model	Mesh			
	15×2	25×2	35×2	50×2
SPQ4	0.814	0.937	0.978	1.003 (-1.724%)
PIM	–	1.098	–	1.111

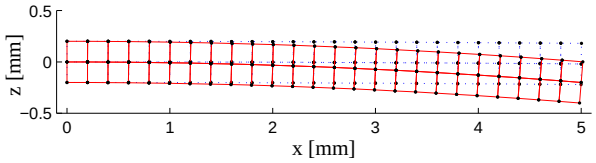

Figure 15: Total deformation of the parallel bimorph cantilever beam.

Liu, G. R., Dai, K. Y., Lim, K. M. and Gu, Y. T. (2002). A point interpolation mesh free method for static and frequency analysis of two-dimensional piezoelectric structures, *Computational Mechanics* **29**: 510–519.

Liu, G. R., Dai, K. Y., Lim, K. M. and Gu, Y. T. (2003). A radial point interpolation method for simulation of twoo-dimensional piezoelectric structures, *Smart Materials and Structures* **12**: 171–180.

Liu, G. R., Dai, K. Y. and Nguyen, T. T. (2007). A smoothed finite element method for mechanics problems, *Computational Mechanics* **39**(6): 859–877.

Liu, G. R., Nguyen, T. T., Dai, K. Y. and Lam, K. Y. (2006). Theoretical aspects of the smoothed finite element method (SFEM), *International Journal for Numerical Methods in Engineering* **(in press)**.

Long, C. S., Loveday, P. W. and Groenwold, A. A. (2006). Planar four node piezoelectric elements with drilling degrees of freedom, *International Journal for Numerical Methods in Engineering* **65**: 1820–1830.

Mackerle, J. (2003). Smart materials and structures - an finite element approach - an addendum: a bibliography (1997-2002), *Modelling and Simulation in Materials Science and Engineering* **11**: 707–744.

Mercer, C. D., Reddy, B. D. and Eve, R. A. (1987). Finite Element Method for Piezoelectric Media, *Technical Report 92*, UCT/CSIR Applied Mechanics Research Unit Technical Report, Univers.

Nguyen-Van, H., Mai-Duy, N. and Tran-Cong, T. (2007). A simple and accurate four-node quadrilateral element using stabilized nodal integration for laminated plates, *CMC: Computers, Materials & Continua* **6**(3): 159–176.

Ohs, R. R. and Aluru, N. R. (2001). Meshless analysis of piezoelectric devices, *Computational Mechanics* **27**: 23–36.

Ray, M. C., Bhattacharya, R. and Samanta, B. (1998). Exact solutions for dynamic analysis of composite plates with distributed piezoelectric layers, *Computers and Structures* **66**(6): 737–743.

Shen, I. Y. (1995). Bending and torsional vibration vibration control of composite beam through intelligent constrained-layer damping treatments, *Smart Materials & Structures* **4**(1): 340–355.

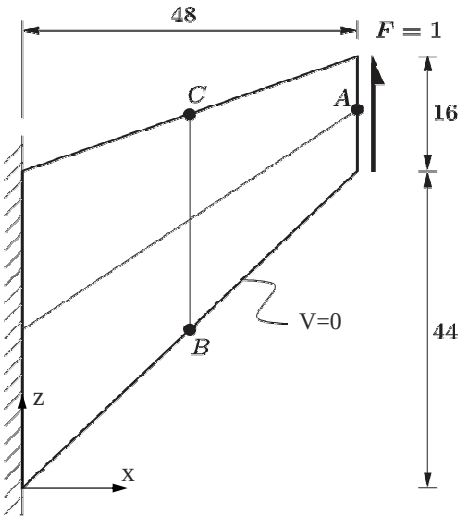

Figure 16: Piezoelectric Cook's membrane.

Table 4: Computed results of piezoelectric membrane and relative error percentage.

Variable	SPQ4				FEM
	4×4	8×8	16×16	24×24	
$u_{zA} \times 10^{-4}(mm)$	1.880	2.042	2.091	2.100	2.109
	(-10.858%)	(-3.177%)	(-0.853%)	(-0.379%)	
$\phi_A \times 10^{-8}(GV)$	1.270	1.579	1.680	1.703	1.732
	(-26.674%)	(-8.834%)	(-3.002%)	(-1.674%)	
$\sigma_{1B}(N/mm^2)$	0.1578	0.1940	0.2074	0.2109	0.21613
	(-26.978%)	(-10.227%)	(-4.026%)	(-2.406%)	
$D_{1C}(pC/mm^2)$	10.555	16.648	19.785	20.754	22.409
	(-52.898%)	(-25.708%)	(-11.709%)	(-7.385%)	

Sladek, J., Sladek, V., Zhang, C., Garcia-Sanche, F. and Wunsche, M. (2006). Meshless Local Petrov-Galerkin Method for Plane Piezoelectricity, *CMC: Computers, Materials & Continua* **4**(2): 109–117.

Sladek, J., Sladek, V., Zhang, C., Solek, P. and Starek, L. (2007). Fracture Analyses in Continuously Nonhomogeneous Piezoelectric Solids by the MLPG, *CMES: Computer Modeling in Engineering & Sciences* **19**(3): 247–262.

Sze, K. and Pan, Y. (1999). Hybrid finite element models for piezoelectric materials, *Journal of Sound and Vibration* **226**: 519–547.

Sze, K., Yang, X.-M. and Yao, L.-Q. (2004). Stabilized plane and axisymmetricpiezoelectric finite element models, *Finite Elements in Analysis and Design* **40**: 1105–1122.

Sze, K. and Yao, L. (2000). Modelling smart structures with segmented piezoelectric sensors and actuators, *Journal of Sound and Vibration* **235**: 495–520.

Tzou, H. S. and Tiersten, H. F. (1994). Elastic analysis of laminated composite plates in cylindrical bending due to piezoelectric actuators, *Smart Materials and Structures* **3**: 255–265.

Wu, C., Sze, K. and Huang, Y. (2001). Numerical solutions on fracture of piezoelectric materials by hybrid element, *International Journal of Solids and Structures* **38**: 4315–4329.

Zemcik, R., Rolfes, R., Rose, M. and Temer, J. (2007). High-performance four-node shell element with piezoelectric coupling for the analysis of smart laminated structures, *International Journal for Numerical Methods in Engineering* **70**: 934–961.

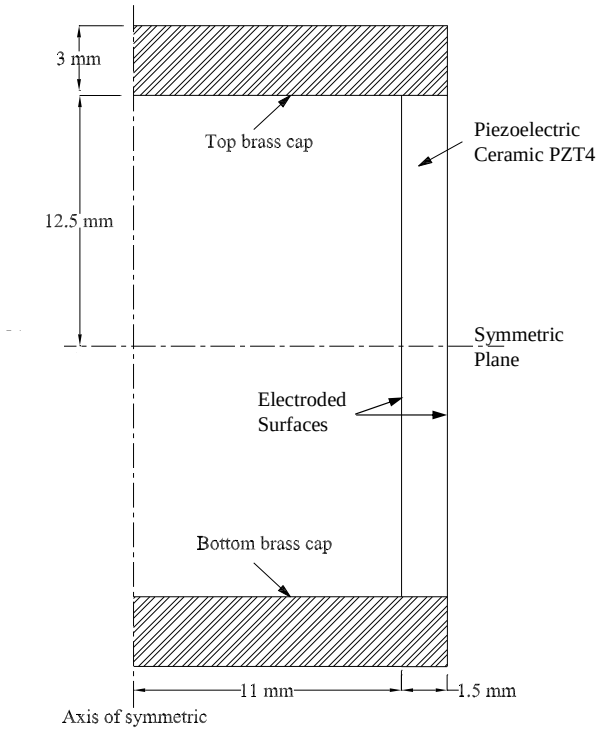

Figure 17: Representative sketch of a transducer.

Table 5: Computed eigenvalues of the transducer and comparison with other solutions.

Model	Mode 1	Mode 2	Mode 3	Mode 4	Mode 5
Experimental	18.6	35.4	54.2	63.3	88.8
PIM (44 cells)	19.9	42.8	59.7	66.1	88.4
	(6.989%)	(20.904%)	(10.148%)	(4.423%)	(-0.450%)
SPQ4 (44 elements)	18.214	41.773	58.642	65.798	87.386
	(-2.075%)	(18.003%)	(8.195%)	(3.946%)	(-1.592%)

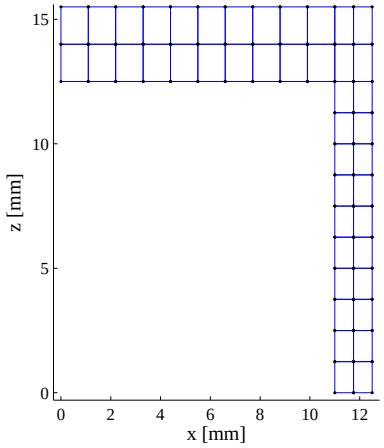

Figure 18: Domain discretization of a transducer.

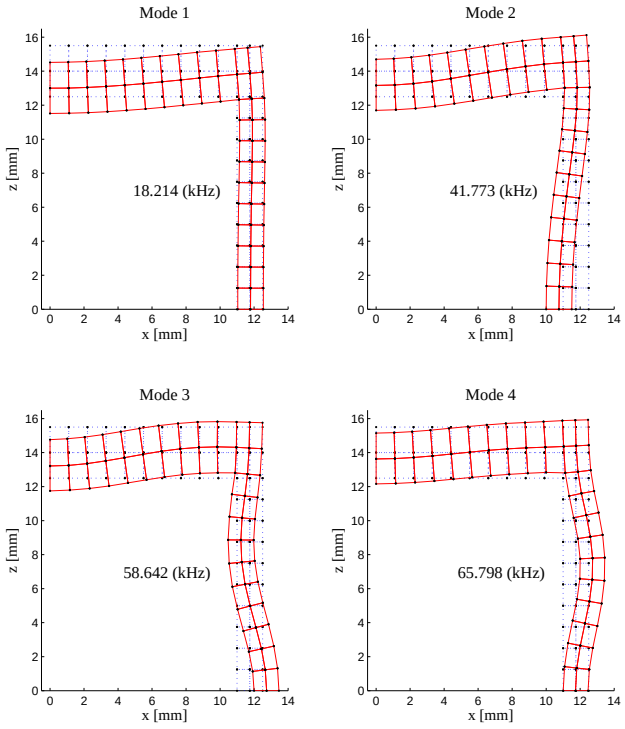

Figure 19: Eigenmodes of the piezoelectric transducer.